Chemical Engineering Journal 207–208 (2012) 497–503

Contents lists available at SciVerse ScienceDirect

Chemical Engineering Journal

journal homepage: www.elsevier.com/locate/cej

Physicochemical changes in *Miscanthus* ash on agglomeration with fluidized bed material

Rudy Michel [a], Judit Kaknics [a], Marie Laure Bouchetou [a], Bernard Gratuze [b], Michael Balland [a], Julien Hubert [a], Jacques Poirier [a,*]

[a] *CEMHTI, CNRS UPR 3079/Université d'Orléans, 1D Avenue de la Recherche Scientifique, 45071 Cedex 2, France*
[b] *Institut de Recherches sur les Archéomatériaux, Centre Ernest Babelon, UMR 5060, Université d'Orléans – CNRS, 3D, rue de la Férollerie, F-45071 Orléans Cedex, France*

HIGHLIGHTS

- The Chemical Fractionation Analysis allows studying the ashes in *Miscanthus*.
- The olivine agglomerates to the molten ash by chemical interaction.
- The calcined olivine has a heterogeneous structure composed of magnetite veins.
- At high temperature, the fayalite transforms into hematite and magnetite.
- During calcination, iron oxide spreads through the olivine surface

ARTICLE INFO

Article history:
Available online 17 July 2012

Keywords:
Miscanthus X giganteus
Ash
Olivine
Agglomeration
Leaching
Iron diffusion

ABSTRACT

Biomass gasification is more suitable than combustion for Combined Heat and Power (CHP) applications. In this field, fluidized bed reactor technology ensures good mixing of continuously fed fuel and provides homogeneous temperature distribution in the reactor. The aim of the gasification is to produce clean syngas, thus it is important to investigate the influence of various operating conditions on the property of gas products and tar evolution. Usually, temperature and catalytic bed composition are the most studied parameters. In spite of the advantages of fluidized beds, biomass gasification suffers from technical problems such as slagging and fouling due to the high ash content and the formation of low melting point compounds and eutectic composition. The understanding of bed agglomeration requires the investigation of natural phases of biomass mineral matter and bed material. Due to the abundance of ash in biomass and its low degree of crystallization, supplementary methods have to be used beside XRD, LA-ICP-MS and SEM–EDX analysis to characterise interactions between ashes and fluidized bed material.

© 2012 Elsevier B.V. All rights reserved.

1. Introduction

Biomass is one of the most promising renewable and clean energy sources; among other plants, corn and sugar cane have been used for decades to produce energy and biofuels. However, because of the emerging concerns about food competitiveness, new non-food resources have to be exploited.

Miscanthus X giganteus (MXG) is a commercially planted grassy energy crop which has remarkable adaptability to different soils and environments; therefore it is suitable for cultivation in Europe and North America [1]. Moreover, MXG has zero net CO_2 emission during growth, and a low water requirement (270–300 l/kg/year). It is sterile, without hazardous proliferation, and it can be cultivated in different kinds of soils ($5.5 < pH < 8$) [2]. The crops showed high yield (>20 tons Ha^{-1} of dry matter) [1], and in addition MXG has a good calorific heating power (16400 kJ kg^{-1}, 1 toe = 2.5 t MXG) [3]. Among other things, the composition of MXG depends on its harvesting season; it contains less ash, alkali metals and moisture if harvested in late winter/early spring compared to autumn [4].

Thermochemical processes provide an attractive solution for biomass conversion to produce electricity and heat. Gasification is the partial oxidation of biomass at 750–900 °C [5]; it converses energy in combustible product gases. The main products are CO and H_2, besides these, condensable and volatile hydrocarbons, coke, CO_2, CH_4 are formed. Gasifiers can be classified via their gas–solid contacting mode into three main types; fixed bed, fluidized bed and entrained flow gasifiers [6–8]. Each type is suitable for a given capacity, namely fixed bed gasifiers are used in 10 kWth–10 MWth units, while fluidized beds are more suitable for medium scale between 5 MWth and 100 MWth and entrained flow gasifiers for large scale applications (>50 MWth) [8,9]. The two main types of fluidized bed reactors are circulating and bubbling fluidised beds [7]. In fluidized bed reactors, the bed

---

* Corresponding author. Tel.: +33 238255514; fax: +33 238638103.
E-mail address: jacques.poirier@univ-orleans.fr (J. Poirier).

1385-8947/$ - see front matter © 2012 Elsevier B.V. All rights reserved.
http://dx.doi.org/10.1016/j.cej.2012.06.159

material is kept in fluidized state by the gasifying medium, which serves as a heat reservoir during the thermochemical process and it helps to achieve homogenous temperature distribution and adequate material mixing in the reactor [8].

Olivine (Mg, Fe)$_2$SiO$_4$ is used as bed material for its catalytic effect and promotes gas formation by tar decomposition [8].

The disadvantage of fluidised beds is the risk of agglomeration. Bed material can react with alkalis from ashes and form new compounds with low melting point (500–1000 °C) resulting in molten ash which acts like glue between bed particles causing agglomeration [8,10]. Therefore, agglomeration highly depends on the process temperature: the higher the temperature in the reactor the more likely the agglomeration is [11,12]. The temperature gradient between a fuel particle and bed particle is also substantial as it can promote the transfer of volatized alkali from fuel to bed particle [10]. In bubbling fluidized beds the two main reverse forces are the adhesive force by sticky ash coating and the breaking force created by bubbles [13]. When adhesive force is higher than breaking force, agglomeration between particles occurs [14]. It depends on the reactor geometry (volume, surface), process conditions, ash chemistry and interaction between ash and bed material, whether agglomeration leads to defluidization or only bed disturbance [15]. Defluidization of the reactor bed can be noticed by a sharp pressure drop and an uneven heat distribution in the reactor [12,16].

Regarding the interaction of ash and bed material, the silica and alkali content of ash is crucial, therefore it is important to know the inorganic content in the plant concentrations of the main ash-forming elements (Si, Al, Fe, Ca, Mg, Mn, Na, K, P, S, and Cl) and the ways they are associated in the organic structures: salts, oxide minerals, and vitreous compounds [17,18]. Inorganics serve different functions in the plant such as stiffening, transport of elements, plant growth regulation, hence they can be found in different forms and concentration in the plant. The initial form of ashes in biomass influences the form after gasification and it determines their concentration in the flue gas and the residue [18].

The aim of this research is to study the risk of agglomeration of MXG ashes with olivine bed material. On the one hand, the paper is focused on the study of evolution of olivine as a function of temperature and the characterisation of MXG ashes by leaching. On the other hand, agglomeration tests are done on mixture of ash and olivine at 900 °C.

This study is integrated in the GAMECO project [19]. The GAMECO project is focused on improving gasification for Combined Heat and Power (CHP) applications.

2. Materials and methods

2.1. *Miscanthus X giganteus*

Two different *Miscanthus X giganteus* (MXG) samples are studied; the first one LM#1 harvested in April 2011 and the second LM#2 harvested in September 2011 (Fig. 1). The lots are supplied by NOVABIUM from La Ferté Chevresis (France).

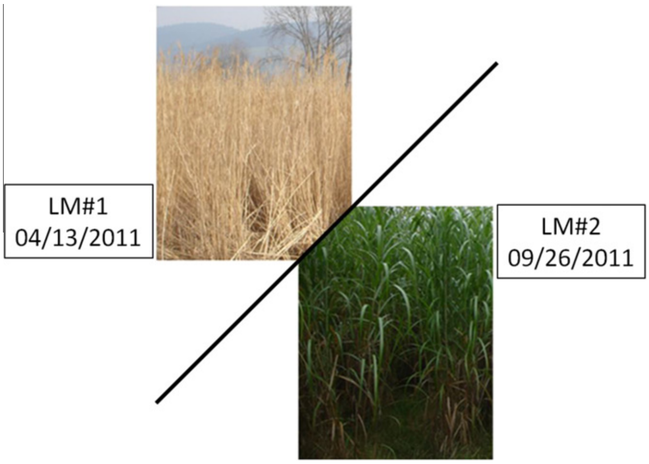

Fig. 1. Plan of *Miscanthus X giganteus* (MXG).

Miscanthus has low ash content. So in a real gasifier, the inorganic part is diluted in the organic part and cannot be analysed. A prior combustion at low temperature allows separating the inorganics from biomass. The aim is to get adequate amount of ashes for the study without influencing the initial phases. Thus, the ashes are prepared by crushing and burning dried *Miscanthus* in a muffle furnace at 400 °C for 8 h in air atmosphere.

2.2. Olivine material

Olivine is an orthosilicate with the general formula of (Mg$_{1-x}$Fe$_x$)$_2$SiO$_4$ (x near 0.1) corresponding to the complete solid solution between forsterite, Mg$_2$SiO$_4$, and fayalite, Fe$_2$SiO$_4$. In fact, the olivine contains Mg$_2$SiO$_4$ as the main phase, with small quantities of its oxidation products: Enstatite MgSiO$_3$.

The material is mined at the Åheim Plant, Norway. It is sieved to obtain particle size between 400 and 500 μm. This olivine will be referred to the initial natural olivine.

As catalyst, it is calcined at 1400 °C in air atmosphere for 4 h (Fig. 2). This initial calcination is used to improve the olivine's mechanical properties for fluidized bed use [20].

2.3. Characterisation of materials

The mass of mineral mater is determined by Thermal Gravimetric Analysis (TGA) on Setaram Setsys Evolution 2400. TGA analysis is done on raw *Miscanthus* stem after crushing. 103 mg of MXG is heated to 550 °C with a heating rate of 5 °C min^{-1} in an oxygen flow of 20 ml min^{-1}.

Differential Scanning Calorimetry (DSC) is done on *Miscanthus* ashes on Setaram Ligne 96. 100 mg of ash is heated to 1500 °C with a heating rate of 5 °C min^{-1} in an argon flow (20 ml min^{-1}).

The elemental composition of ash and olivine composition was determined by Laser Ablation Inductively Coupled Plasma Mass Spectrometry (LA-ICP-MS). Samples were prepared after crushing and pelletization then put in the ablation cell together with the reference standard materials.

The object placed in the ablation cell are sampled by the laser beam, which is generated by a Nd YAG pulsed laser. The laser frequency is quadrupled allowing it to operate in the ultraviolet region at 266 nm. The laser operates at a maximum energy of 3–4 mJ and at a maximum pulse frequency of 15 Hz. The diameter of the ablation crater ranges from 60 μm to 100 μm, and its depth is around 250 μm depending of the ablation duration and the laser pulse frequency. Classical parameters are 70 s of ablation (20 s for pre-ablation and 50 s for analysis) and 6–8 Hz laser pulse frequency. The pre-ablation time of 20 s is set in order to eliminate the transient part of the signal and to ensure that a possible surface contamination or corrosion does not affect the results of the analysis. An argon gas flow carries the ablated aerosol to the injector inlet of the plasma torch, where the matter is dissociated, atomised and ionised (typical flow rate values range from 1.15 l min^{-1} to 1.35 l min^{-1} depending on the cell size). The ions are then injected into the vacuum chamber of a high resolution system, which filters the ions depending upon their mass-to-charge ratio. The ions are then collected by the channel electron multiplier or the Faraday cup.

The crystalline phases were examined by powder X-ray diffraction (XRD) on a Bruker D8 Advance X-ray diffractometer using Cu Kα radiation (λ = 1.5406 Å) with a step size of 0.016°, sample turn at 15 rpm and scan speed of 2 s step^{-1}.

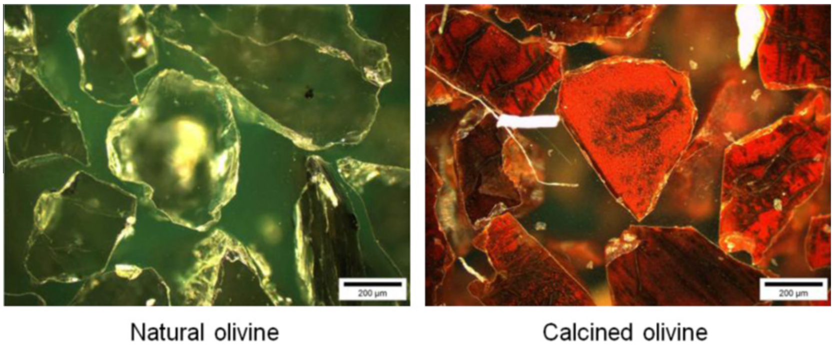

Natural olivine Calcined olivine

Fig. 2. Optical micrographs of natural and calcined olivine.

Due to the weak abundance of ashes in biomass and its low degree of crystallization, XRD and SEM–EDX have to be supported by supplement analytical techniques. Using the Chemical Fractionation Analysis (CFA) test method, the distribution of inorganics in different form can be determined, from which conclusion of their reactivity during gasification can be drawn [18]. The CFA test is based on the sequential extraction of inorganics from samples in ultrapure water, ammonium acetate and finally in hydrochloric acid. Water soluble inorganics are present as ions in the plant, while acetate soluble elements are associated to organics, such as oxalic acid. Elements belonging to these two groups are in reactive form; they volatilise and react with each other or with silicates in gas phase forming low melting point compounds [18].

The CFA procedure in this work is done on crushed *Miscanthus* (LM#1). About 70 g of dry sample was transferred to a 500 ml PE flask and sequentially leached:

(1) Samples A, B, C; once in 400 ml ultra-pure H_2O for 24 h under turbula mixer.
(2) Samples B, C; once times in 400 ml 1.0 M $NH_4Ac(aq)$ for 24 h under turbula mixer.
(3) Sample C; once in 400 ml 1.0 M HCl(aq) for 24 h under turbula mixer.

After each leaching step (in water, buffer, and acid), the solids were rinsed two times with 500 ml ultra-pure water and dried for 48 h at 80 °C. In order to determine the remaining mineral matter, samples are burned in a muffle furnace at 400 °C and pelletized. The samples are analysed by X-ray Diffraction (XRD) then the elemental composition is determined by LA-ICP-MS with alumina used for reference.

2.4. Interactions ashes/olivine

To characterise the ash-bed material interaction, ash (LM#1) and crude/calcined olivine was loosely mixed in platinum crucible and samples were heat treated for 6 h at 900 °C in muffle furnace. The samples were observed to study the morphology and to measure the composition profiles in the bulk on cut grains. For this purpose, the samples were embedded in an epoxy resin, polished in order to obtain planar and smooth surfaces and finally coated with gold in order to be examined by SEM–EDX (FEG Hitachi S4500).

3. Results and discussions

3.1. Analysis of olivine

LA-ICP-MS analysis is done on an olivine sample which was formerly crushed and pressed for homogenisation. Results are presented in Table 1 in terms of elements and in terms of corresponding oxide phases.

Olivine is an iron and magnesium silicate with trace elements as Ni, Al and Cr. The molar ratio Mg/Fe is 11.7; so the olivine formula is defined as $(Mg_{0.92}, Fe_{0.08})_2SiO_4$.

X-ray diffraction (Fig. 3) shows that forsterite Mg_2SiO_4 is the main phase. In addition, the second observed phase is enstatite $MgSiO_3$ visualised at $2\theta = 28.1°$ and $31.2°$. Crude olivine also contains clino-enstatite ($2\theta = 31.3°$). According to Reynard et al. clino-enstatite transforms into proto-enstatite at high temperature [21].

Afterwards, serpentine $Mg_3Si_2O_5(OH)_4$ phase disappear during calcination due to dehydration according to the following reactions:

$$2Mg_3Si_2O_5(OH)_4 \rightarrow 2Mg_2SiO_4 + 2MgSiO_3 + 4H2O \tag{1}$$

For the calcined olivine, the spinel phase can be observed. Where, fayalite Fe_2SiO_4 oxidation leads to iron oxide according to the following reactions:

$$2Fe_2SiO_4 + O_2 \rightarrow 2Fe_2O_3 + 2SiO_2 \tag{2}$$

$$3Fe_2SiO_4 + O_2 \rightarrow 2Fe_3O_4 + 3SiO_2 \tag{3}$$

Then quartz SiO_2 reacts with forsterite to form enstatite according to the following reactions:

$$Mg_2SiO_4 + SiO_2 \rightarrow 2MgSiO_3 \tag{4}$$

3.2. Analysis of Miscanthus X giganteus

TGA and DSC curves of *Miscanthus* are presented in Figs. 4 and 5 respectively. Concerning LM#1, 2.7 wt.% of ash on Dry Matter (DM) is determined at 550 °C and only 1.8 wt.% of ash in case of LM#2.

The high ash content of LM#1, harvested in April is caused by leaf senescence and reduction of leaf area [22]. Moreover only stems are burned, therefore the ash content of the LM#2 leaves is not considered in the calculation.

According to Kahle et al., the *Miscanthus* leaves are characterised by a gradual senescence which means that the basal leaves

Table 1
Composition of olivine (wt.%) by LA-ICP-MS analysis.

Oxides (%)		Elements (%)	
SiO_2	45.3	Si	21.2
MgO	45.3	Mg	23.3
Fe_2O_3	7.7	Fe	5.4
Al_2O_3	0.6	Al	0.3
CaO	0.1	Ca	0.1
Cr_2O_3	0.4	Cr	0.3
MnO	0.1	Mn	0.1
NiO	0.4	Ni	0.3

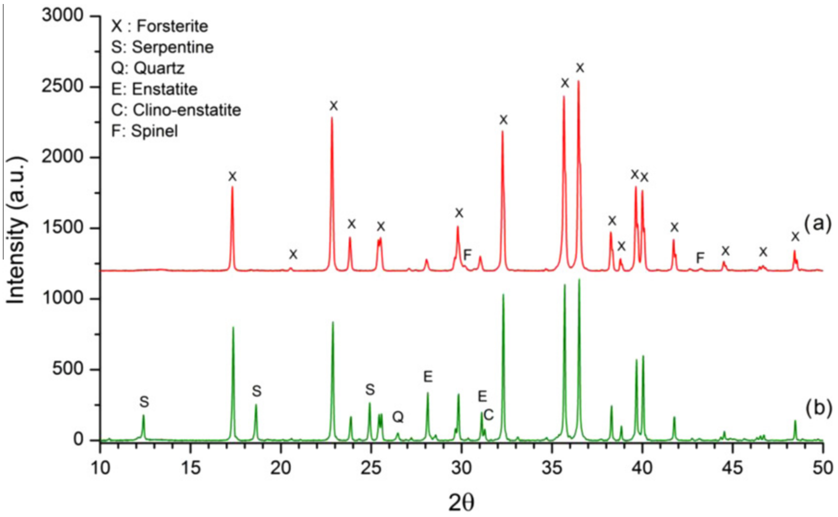

Fig. 3. Diffractograms of natural olivine (b) and calcined olivine (a) at 1400 °C.

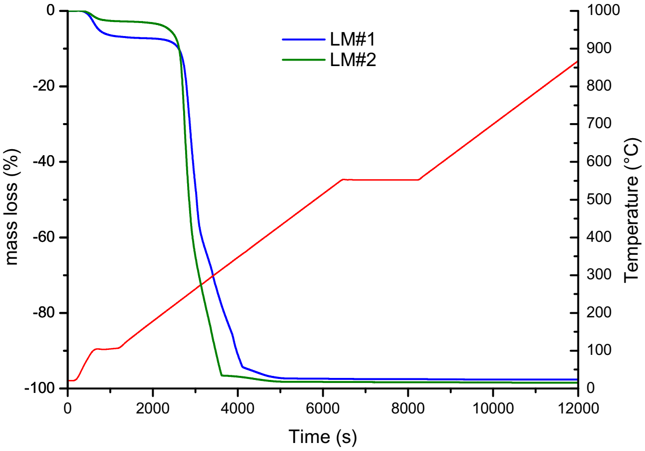

Fig. 4. TGA of MXG in O_2 (LM#1 and LM#2).

start to die at the beginning of July. The shoot-tips stay alive until the first frosts at the end of vegetation period [23].

During winter, most of the leaves and the non-woody tops fall off the *Miscanthus* plant [1].

Weather conditions have strong influence on biomass quality. Following senescence, Cl, K and ash components are leached from the shoots.

DSC curves reveal that overall the ash samples have endothermic response. The endothermic peak occurring at 635 and 750 °C incarnates phase transition. The last reaction corresponds to the temperature of liquidus (fusion of ash) at 1410 °C due to high content of silica (Table 2), which is the main reaction of the whole melting process. The endothermic peaks at 750 °C correspond to the melting point of KCl salt.

LA-ICP-MS analysis results of *Miscanthus* ash are presented in Table 2.

Both *Miscanthus* ash samples (LM#1 and LM#2) are mainly composed of Si, K, Ca, Mg, P and Cl. A higher content of K, P and Cl in case of LM#2 shows the possibility to get potassium chloride and phosphate. Sulphur and nitrogen cannot be detected by the LA-ICP-MS method, but their presence is possible. The high Si, K, Ca and Mg content points to the possibility of glass formation at high temperature.

Table 2
Composition (wt.%) of MXG ashes from spring harvest (LM#1) and autumn harvest (LM#2).

LM#1				LM#2			
Oxides (%)		Elements (%)		Oxides (%)		Elements (%)	
SiO_2	56.2	Si	43.6	SiO_2	37.2	Si	25.6
K_2O	27	K	37.2	K_2O	48.6	K	59.5
CaO	8.7	Ca	10.3	CaO	3.1	Ca	3.3
MgO	3.2	Mg	3.2	MgO	2.3	Mg	2.1
P_2O_5	2.5	P	1.8	P_2O_5	4	P	2.6
Cl	2.7	Cl	3.6	Cl	4.6	Cl	6.8
Na_2O	0.1	Na	0.2	Na_2O	0.1	Na	0.1
Traces	0.2	Traces	0.1	Traces	0.01	Traces	0.005

Traces: Mn, Ba, Zn, Sr, Cu, B, Ti, Fe.

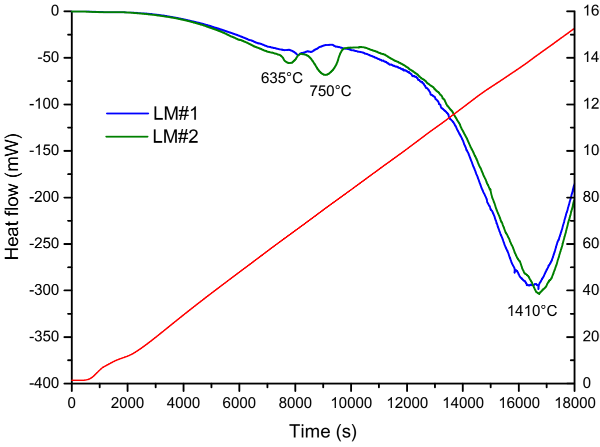

Fig. 5. DSC of MXG in Ar (LM#1 and LM#2).

Figs. 6 and 7 respectively show the results of LA-ICP-MS and XRD after the Chemical Fractionation Analysis (CFA) protocol on LM#1.

The analysis shows the results obtained with MXG sample before CFA protocol for comparison and the typical percentages of each element after leaching with water (Sample A), buffer (Sample B), and acid (Sample C) normalised on alumina reference. It is important to recall that insoluble silicates remain in the sample.

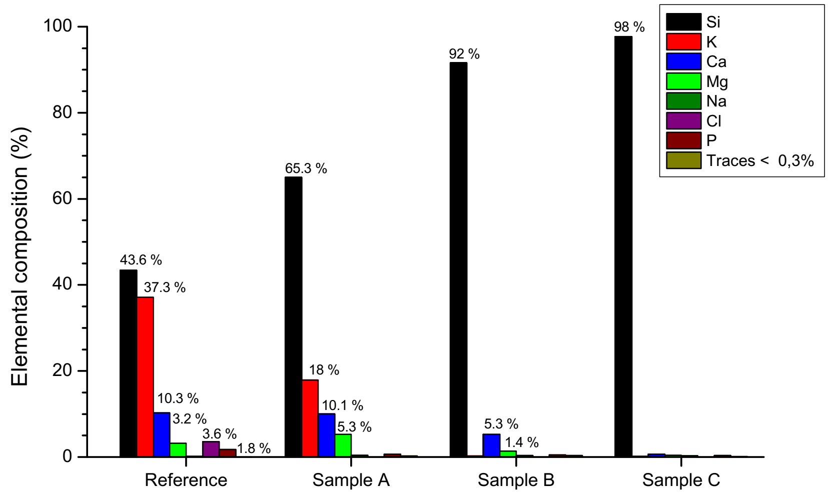

Fig. 6. LA-ICP-MS analysis of MXG leaching (wt.%): (Sample A) leaching with water; (Sample B) leaching with ammonium acetate; (Sample C) leaching with hydrochloric acid.

Thus, we can compare results of LA-ICP-MS considering the Si element constant.

After leaching with water (Fig. 6), the amounts of K, P and Cl decreases significantly, that leads to conclude that these elements are present as different salts. After leaching with ammonium acetate, the concentrations of Ca and Mg decrease and there is also some loss of K. These elements are connected to organic species in the *Miscanthus*. After the final step, all elements, excluding Si, almost totally disappear. The small quantity of remaining alkalines is in the form of non-soluble silicates.

Fig. 7 shows the XRD diffractogram obtained by the CFA procedure. The presence of amorphous phase before and after the leaching procedure is due to the high content of silica.

The diffractograms of the reference and samples A, B, C together provide more complex information of the different crystalline phases in the ash. After leaching, the diffractograms have less and better differentiated peaks due to the clearance of some disturbing and overlapping phases and the appearance of so far hidden components.

The difference between the diffractograms of sample A and reference reveals the presence of salts, mainly KCl and K_2SO_4, and probably the presence K_2HPO_4 and $Ca_3(PO_4)_2$. These salts, soluble in water, disappear after water leaching. In the case of the difference between diffractograms of samples A and B, $CaCO_3$ is identified after the exchange of Ca^{2+} by NH_4^+, as a consequence of leaching by ammonium acetate. Sample B still contains a small amount of $CaCO_3$ because of incomplete leaching. The diffractogram of Sample C after leaching with HCl presents only an amorphous phase composed of SiO_2 shown by LA-ICP-MS.

3.3. Interactions between ashes and olivine

Ash (LM#1) and bed material interaction are studied by SEM–EDX (Figs. 8 and 9). Olivine particles (dark areas) surrounded by molten ash can be observed. First, it is worth noting that, after interaction at 900 °C, calcined olivine presents veins on its surface (Fig. 8) contrary to natural olivine (Fig. 9) due to the calcination at 1400 °C where iron is exalted. These veins have an iron oxide in high content. Iron oxide is also present on the surface of grain in contact with the molten ashes. This white layer at 18 μm contains 20% of Fe and 16.8% of K. The next point at 19 μm contains 9.2% of Fe and 20.5% of K, and then the point at 29 μm contains 0.6% of Fe and 21.1% of K.

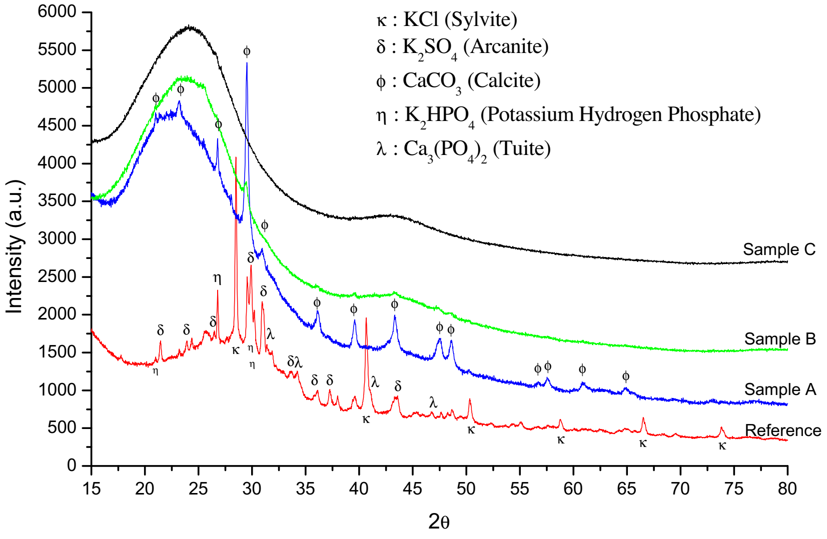

Fig. 7. XRD diffractogram of MXG leaching: (Sample A) leaching with water; (Sample B) leaching with ammonium acetate; (Sample C) leaching with hydrochloric acid.

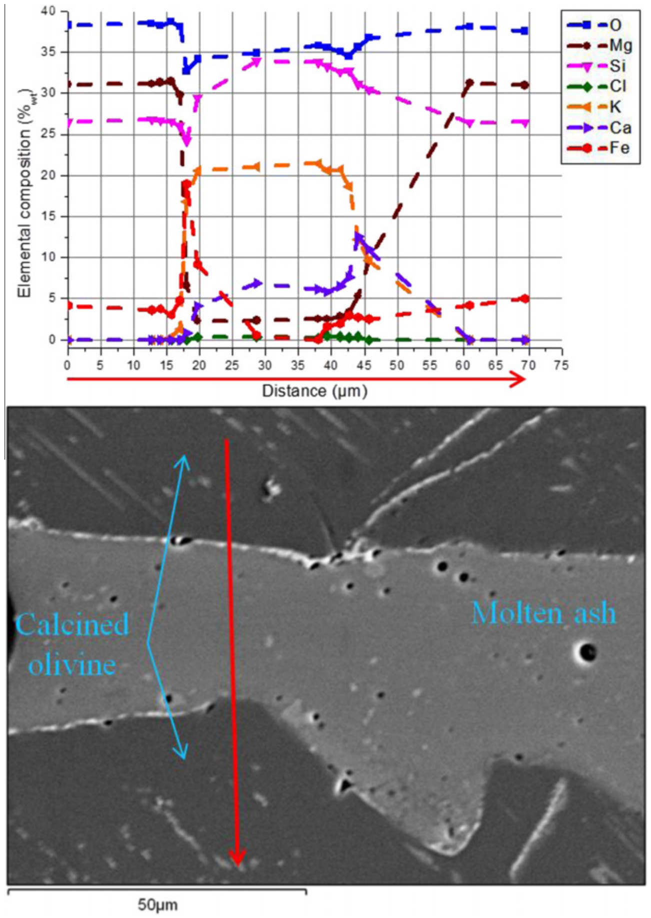

Fig. 8. MEB–EDX analysis of the interactions between molten ash and calcined olivine.

We can suppose that there is a diffusion of iron from calcined olivine to molten ash at high temperature, showing a chemical interaction, which contributes to the agglomeration, while MXG ashes contain only traces of iron (<0.1%).

In the case of interaction with crude olivine, iron is found in low content (3.2% of Fe and 21.3% of K) in molten ash on olivine surface. Iron is not exalted by calcination at 1400 °C and the diffusion through natural olivine to molten ash at high temperature is lower than through calcined olivine.

Considering MXG ashes of LM#2 harvested in autumn, agglomeration phenomena will be more important due to the high content of potassium as it is shown in Table 2.

4. Conclusions

To be able to understand the agglomeration phenomena in bubbling fluidized bed gasifiers, it is important to study the inorganic composition of bed material and biomass ash first. In this study, the composition of olivine and two types of *Miscanthus* ashes deriving from different harvest have been investigated.

It was found that harvested season influences ash characteristics. *Miscanthus* harvested in May had a higher ash content when harvested in October, but the concentration of potassium, chloride and phosphate in the ash was lower in spring than in autumn.

The elemental composition of ash was analysed by solid LA-ICP-MS. This method is interesting but not sufficient to describe different chemical phases. The main contributors in ash are Si, K, Ca, Mg, P and Cl.

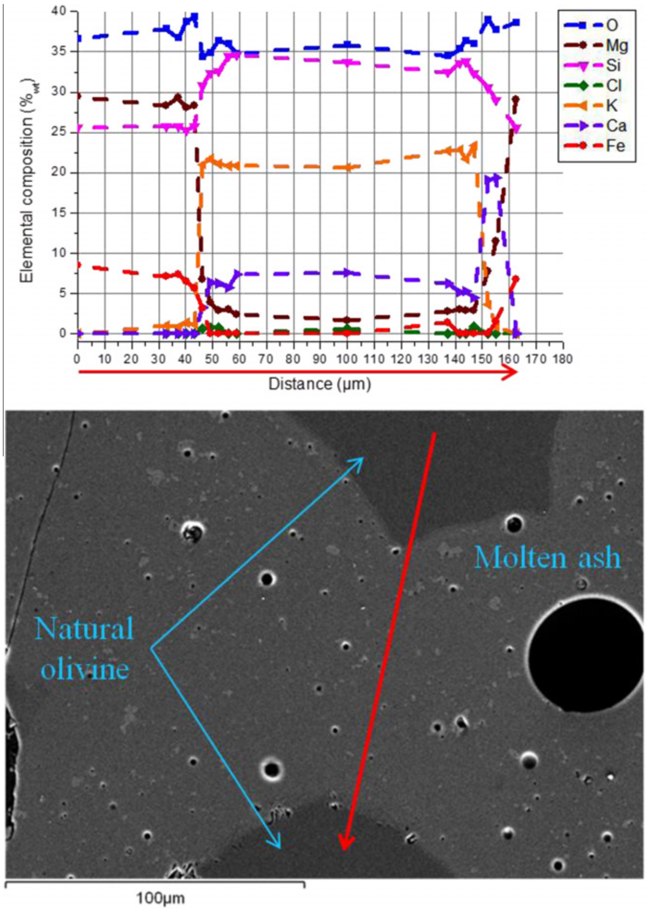

Fig. 9. MEB–EDX analysis of the interactions between molten ash and crude olivine.

XRD analysis of MXG ashes after leaching by Chemical Fractionation Analysis completes the LA-ICP-MS analysis. Different phases were determined such as KCl, K_2SO_4, K_2HPO_4, $CaCO_3$ and amorphous SiO_2 is also present.

The DSC analysis shows endothermic peaks between 635 and 750 °C corresponding to a polymorphic transition in the ashes. The temperature of liquidus is 1410 °C due to high content of silica.

Natural olivine composed of $(Mg_{0.92}, Fe_{0.08})_2SiO_4$ transforms at high temperature by dehydration and oxidation of iron.

SEM analysis permitted visualising the interaction between ash and bed material. Analysing the surface of heat-treated samples showed that there is a thin layer of iron containing ash around the bed particle. This points to the fact that iron participate in layer formation via diffusion from the inner part of the olivine grain to the surface.

Acknowledgement

We thank the ANR (Agence Nationale de la Recherche) for funding these projects.

References

[1] I. Lewandowski, J.C. Clifton-brown, J.M.O. Scurlock, W. Huisman, *Miscanthus*: European experience with a novel energy crop, Biomass Bioenergy 19 (2000) 209–227.

[2] J.J. Villaverde, R.M.A. Domingues, C.S.R. Freire, A.J.D. Silvestre, C. Pascoal Neto, A. Ligero, et al., *Miscanthus X giganteus* extractives: a source of valuable phenolic compounds and sterols, J. Agric. Food Chem. 57 (2009) 3626–3631.

[3] M. Bartels, J. Nijenhuis, J. Lensselink, M. Siedlecki, W. de Jong, F. Kapteijn, et al., Detecting and counteracting agglomeration in fluidized bed biomass combustion, Energy Fuels 23 (2009) 157–169.

[4] E.M. Hodgson, D.J. Nowakowski, I. Shield, A. Riche, A.V. Bridgwater, J.C. Clifton-Brown, et al., Variation in *Miscanthus* chemical composition and implications for conversion by pyrolysis and thermo-chemical bio-refining for fuels and chemicals, Bioresour. Technol. 102 (2011) 3411–3418.
[5] P. Basu, Biomass gasification and pyrolysis: gasification theory and modelling of gasifiers chapter 3 pyrolysis and torrefaction, first ed., Elsevier Inc., 2010.
[6] R. Michel, S. Rapagnà, M. Di Marcello, P. Burg, M. Matt, C. Courson, et al., Catalytic steam gasification of *Miscanthus X giganteus* in fluidised bed reactor on olivine based catalysts, Fuel Process. Technol. 92 (2011) 1169–1177.
[7] P. McKendry, Energy production from biomass (part 3): gasification technologies, Bioresour. Technol. 83 (2002) 55–63.
[8] P. Basu, Biomass gasification and pyrolysis: gasification theory and modelling of gasifiers chapter 6 design of biomass gasifiers, first ed., Elsevier Inc., 2010. (ISBN:978-0-12-374988-8).
[9] A.F. Kirkels, G.P.J. Verbong, Biomass gasification: still promising? A 30-year global overview, Renew Sustain Energy Rev 15 (2011) 471–481.
[10] T. Liliedahl, K. Sjöström, K. Engvall, C. Rosén, Defluidisation of fluidised beds during gasification of biomass, Biomass Bioenergy (2011), http://dx.doi.org/10.1016/j.biombioe.2011.05.006.
[11] S. Li, L. Shang, H. Teng, Q. Lu, A model for agglomeration in bio-fuel fired fluidized bed, J. Therm. Sci. 19 (2010) 451–458.
[12] G. Olofsson, Z. Ye, I. Bjerle, A. Andersson, Bed agglomeration problems in fluidized-bed biomass combustion, Ind. Eng. Chem. Res. 41 (2002) 2888–2894.
[13] B.-M. Steenari, A. Lundberg, H. Pettersson, M. Wilewska-Bien, D. Andersson, Investigation of ash sintering during combustion of agricultural residues and the effect of additives, Energy Fuels 23 (2009) 5655–5662.
[14] W. Pietsch, Agglomeration in industry-occurrence and application, vol. 1, Wiley-VCH Verlag GmbH & Co., 2005. (ISBN:978-3-527-30582-7).
[15] M. Zevenhoven-onderwater, R. Backman, B. Johan Skrifvars, M. Hupa, The ash chemistry in fluidised bed gasification of biomass fuels. Part I: Predicting the chemistry of melting ashes and ash-bed material interaction, Fuel 80 (2001) 1489–1502.
[16] W. Lin, K. Dam-Johansen, F. Frandsen, Agglomeration in bio-fuel fired fluidized bed combustors, Chem. Eng. J. 96 (2003) 171–185.
[17] J. Werkelin, B.-J. Skrifvars, M. Zevenhoven, B. Holmbom, M. Hupa, Chemical forms of ash-forming elements in woody biomass fuels, Fuel 89 (2010) 481–493.
[18] C. Andrea Jordan, G. Akay, Speciation and distribution of alkali, alkali earth metals and major ash forming elements during gasification of fuel cane bagasse, Fuel 91 (2012) 253–263.
[19] C.W.O. Authier, A.E. Khalfi, S. Kahloul, J.C. Valle-Marcos, L. Dieckhoff, L. Sanchez, Y. Aleman, A. Delebarre, G. Mauviel, A. Dufour, M. Nowakowska, O. Herbinet, P.A. Glaude, Y. Rogaume, P. Girods, J. Poirier, R. Michel, J. Kerhoas, Biomass gasification for combined heat power (CHP) applications: the GAMECO project, in: Nineteenth European Biomass Conference and Exhibition, Berlin, 2011, pp. 1367–1369.
[20] D. Swierczynski, C. Courson, L. Bedel, A. Kiennemann, S. Vilminot, Oxidation reduction behavior of iron-bearing olivines $(Fe_xMg_{1-x})_2SiO_4$ used as catalysts for biomass gasification, Chem. Mater. 18 (2006) 897–905.
[21] B. Reynard, J.D. Bass, J.M. Jackson, Rapid identification of steatite–enstatite polymorphs at various temperatures, J. Eur. Ceram. Soc. 28 (2008) 2459–2462.
[22] J.C. Clifton-brown, B. Neilson, I. Lewandowski, M.B. Jones, The modelled productivity of *Miscanthus X giganteus* (GREEF et DEU) in Ireland, Ind. Crops Prod. 12 (2000) 97–109.
[23] P. Kahle, S. Beuch, B. Boelcke, P. Leinweber, H.-R. Schulten, Cropping of *Miscanthus* in Central Europe: biomass production and influence on nutrients and soil organic matter, Eur. J. Agron. 15 (2001) 171–184.